ChemPubSoc Europe

DOI: 10.1002/open.201800210

ChemistryOPEN Full Papers

Designing Self-Assembled Rosettes: Why Ammeline is a Superior Building Block to Melamine

Andre Nicolai Petelski[a, b] and Célia Fonseca Guerra*[a, c]

In supramolecular chemistry, the rational design of self-assembled systems remains a challenge. Herein, hydrogen-bonded rosettes of melamine and ammeline have been theoretically examined by using dispersion-corrected density functional theory (DFT-D). Our bonding analyses, based on quantitative Kohn–Sham molecular orbital theory and corresponding energy decomposition analyses (EDA), show that ammeline is a much better building block than melamine for the fabrication of cyclic complexes based on hydrogen bonds. This superior capacity is explained by both stronger hydrogen bonding and the occurrence of a strong synergy.

1. Introduction

Owing to their promising applications as self-assembled materials, the use of hydrogen-bonded rosettes as building blocks for large nanostructures has attracted much attention in recent years.[1] These supramolecules are cyclic complexes of small organic compounds that are associated by hydrogen bonds. They play a fundamental role in biology, such as in naturally occurring guanine quartets,[2] but they may also have potential applications in materials science research[3] and nanoelectronics.[4]

Beyond its industrial importance,[5] melamine (M; Scheme 1, black structure, R = NH_2) has been considered a very versatile building block that produces a great diversity of sophisticated functional materials.[6] For example, melamine rosettes can be deposited as self-assembled monolayers (SAMs) over gold[7] or graphite.[8] This molecule is usually covalently modified by replacing one amino group by long alkylic chains with aromatic rings to add van der Waals interactions and, therefore, improve the binding of the supramolecule. The assembled rosettes of these new species are able both to form SAMs with new functionalities[9] and also stack on top of each other to form pillar arrays or long nanowires.[10] In addition, it has been found that these wires can fold to form toroidal nanostructures.[11] The flexibility of this system reflects how important they may be for bottom-up applications in nanotechnology.

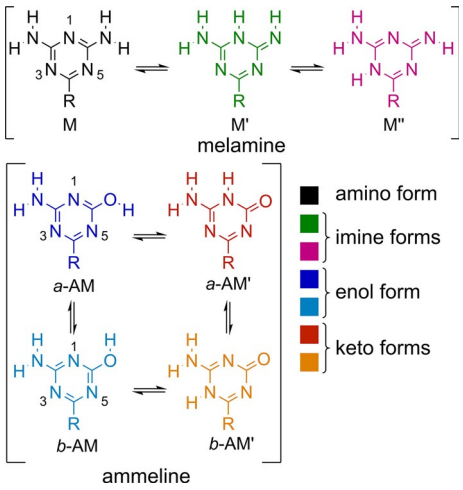

Scheme 1. Molecular structures of isomers that can form rosettes: 1,3,5-triazine-2,4,6-triamine (melamine; M) and 4,6-diamino-1,3,5-triazin-2(1*H*)-one (ammeline; AM).

However, it is known that the sequential hydrolysis of melamine leads to the formation of three related triazine byproducts, namely ammeline (AM, see Scheme 1, blue structures, R = NH_2), ammelide, and cyanuric acid. Of these compounds, rosettes of melamine and cyanuric acid (1:1) are widely known. However, to the best of our knowledge, there is no actual report of hydrogen-bonded rosettes of AM.

With this in mind, we performed computational experiments on hydrogen-bonded rosettes of melamine (M) and ammeline (AM). Because they can undergo amino–imine and keto–enol

[a] *A. N. Petelski, Prof. Dr. C. Fonseca Guerra*
Department of Theoretical Chemistry
Amsterdam Center for Multiscale Modeling, Vrije Universiteit Amsterdam
De Boelelaan 1083, 1081 HV Amsterdam (The Netherlands)
E-mail: c.fonsecaguerra@vu.nl

[b] *A. N. Petelski*
Departamento de Ingeniería Química,
Grupo de Investigación en Química Teórica y Experimental (QuiTEx)
Facultad Regional Resistencia, Universidad Tecnológica Nacional
French 414, H3500CHJ, Resistencia, Chaco (Argentina)

[c] *Prof. Dr. C. Fonseca Guerra*
Leiden Institute of Chemistry, Gorlaeus Laboratories
Leiden University (The Netherlands)

Supporting Information and the ORCID identification number(s) for the author(s) of this article can be found under: https://doi.org/10.1002/open.201800210.

tautomerisms,[12] respectively, our studies considered all the tautomers of these species that could form rosettes (Scheme 1), as shown in Schemes 2 and 3 (R = H). Herein we show that AM could be a more appropriate compound to synthesize hydrogen-bonded supramolecular systems. Our investigations are based on dispersion-corrected density functional theory (DFT-D) in the framework of Kohn–Sham molecular orbital (MO) theory[13] and supported by the corresponding energy decomposition analysis[14] (EDA) and Voronoi deformation density (VDD) analysis of the charge distribution.[15] We examined rosettes in the gas phase and in aqueous solution.

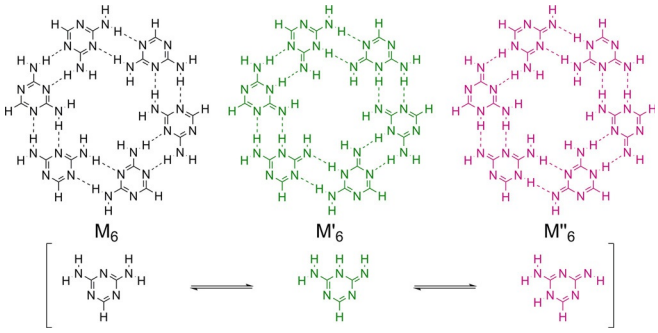

Scheme 2. Molecular structures of M rosettes and monomeric units.

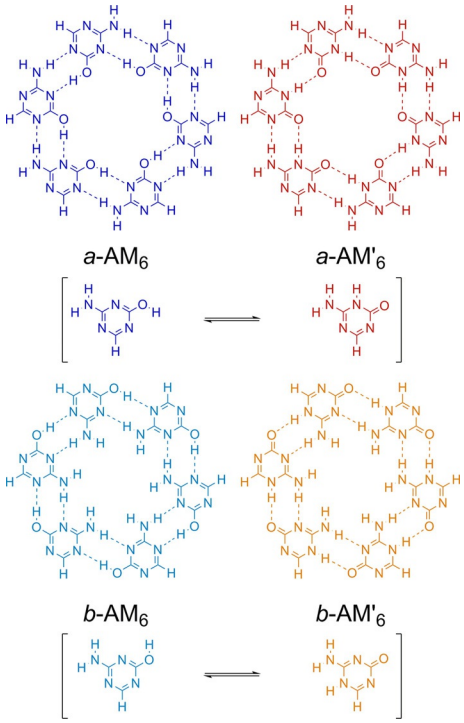

Scheme 3. Molecular structures of AM rosettes and monomeric units.

Computational Details

General Procedure

All calculations were performed by using the Amsterdam Density Functional (ADF) program developed by Baerends et al.,[16] based on dispersion-corrected relativistic DFT at the ZORA-BLYP-D3(BJ)/TZ2P level for geometry optimizations and energies,[17] which has been shown to reproduce hydrogen bond strengths and structures accurately.[18] The basis set superposition error was not computed because the functional has been developed such that it is essentially free of this effect.[17b] To mimic either a surface environment or a stacking arrangement, planar symmetry (C_s) was imposed on all the rosettes. This approach also provides a clear σ–π separation, which is more informative.

It is known that solvents can affect the tautomeric equilibrium.[19] In addition, because recognition and assembly processes in aqueous media are still challenging issues for chemists and water is considered an excellent green solvent,[20] solvent effects in this medium have been estimated by using the conductor-like screening model[21] (COSMO), as implemented in the ADF program.

Bonding Energy Analysis

The energy of formation of the rosette (E_f) is defined according to Equations (1) and (2):

$$\Delta E_f = E_R - 6\,E_m \quad (1)$$

$$\Delta E_f = (E_R - 6\,E_m^*) + [6\,(E_m^* - E_m)] = \Delta E_{bond} + \Delta E_{taut} \quad (2)$$

in which E_R is the energy of the rosette with C_1 symmetry and E_m is the energy of the most stable tautomer conformation of the isolated monomer (Scheme 4). ΔE_{taut} is the energy required for tautomerization ($E_m^* - E_m$).

The bonding energy of the planar system with C_s symmetry is defined in Equation (3):

$$\Delta E_{bond}^{C_s} = \Delta E_{bond} + \Delta E_{C_1 \to C_s} \quad (3)$$

in which $\Delta E_{C_1 \to C_s}$ is the planarization energy (that is, $E_R^{C_s} - E_R$), that is, the energy needed to go from the global minimum of the rosette to the planar, C_s-symmetric structure.

The overall planar bond energy is made up of two major components [Eq. (4)]:

$$\Delta E_{bond}^{C_s} = \Delta E_{prep} + \Delta E_{int} \quad (4)$$

In this equation, the preparation energy (ΔE_{prep}) is the amount of energy required to deform the separate tautomers from their equilibrium structure to the geometry that they acquire in the planar rosette. The interaction energy (ΔE_{int}) corresponds to the actual energy change when the prepared units are combined to form rosettes.

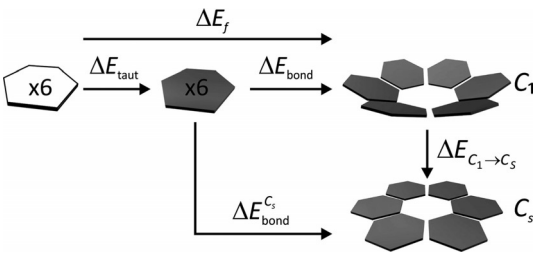

Scheme 4. Partition of the bond energy of rosettes (monomers are indicated by hexagons).

All the interaction energy terms were examined in the framework of the Kohn–Sham MO model by using a quantitative EDA[14] into electrostatic interactions, Pauli-repulsive orbital interactions, and attractive orbital interactions [Eq. (5)].

$$\Delta E_{int} = \Delta V_{elstat} + \Delta E_{Pauli} + \Delta E_{oi} + \Delta E_{disp} \quad (5)$$

The term ΔV_{elstat} corresponds to the classical electrostatic interaction between the unperturbed charge distributions of the prepared (that is, deformed) units and is usually attractive. The Pauli repulsion (ΔE_{Pauli}) is comprised of the destabilizing interactions between occupied orbitals and is responsible for any steric repulsion. The orbital interaction (ΔE_{oi}) accounts for charge transfer (that is, donor–acceptor interactions between occupied orbitals on one moiety and unoccupied orbitals on the other, including HOMO–LUMO interactions) and polarization (empty/occupied orbital mixing on one fragment due to the presence of another fragment). The ΔE_{disp} term accounts for dispersion corrections. The orbital interaction energy can be further decomposed into the contributions from each irreducible representation Γ of the interacting system [Eq. (6)].

$$\Delta E_{oi} = \Delta E_{\sigma} + \Delta E_{\pi} \quad (6)$$

The cooperativity of the hydrogen-bonded rosettes is quantified by comparing ΔE_{int} (that is, the formation of rosettes from their prepared units) with ΔE_{sum}, the sum of the individual pairwise interactions for all possible pairs of units in the rosette (Scheme 5), defined in Equation (7)]:

$$\Delta E_{sum} = 6\,\Delta E_{pair} + 6\,\Delta E_{diag} + 3\,\Delta E_{front} \quad (7)$$

Here ΔE_{pair} is the interaction between two hydrogen-bonded molecules in the geometry of the rosette, ΔE_{diag} is the interaction between two mutually diagonally oriented molecules, and ΔE_{front} is the interaction between two frontal molecules.

The synergy (ΔE_{syn}) that occurs in the rosette motifs is then defined as Equation (8):

$$\Delta E_{syn} = \Delta E_{int} - \Delta E_{sum} \quad (8)$$

Thus, a negative value of ΔE_{syn} corresponds to a constructive cooperative effect; in other words, the whole is greater than the sum of the parts.

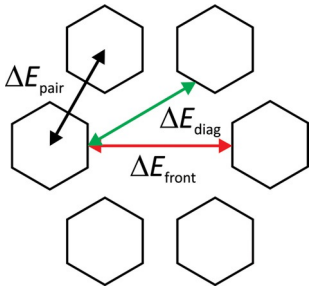

Scheme 5. Definition of interaction energy terms (arrows) in an empty rosette.

2. Results and Discussion

2.1. Structure and Relative Stability

As seen in Schemes 2 and 3, there are different tautomeric forms of M and AM that can form rosettes, and two conformers in the case of AM (*a*-AM and *b*-AM). Each isomeric form determines a unique hydrogen-bonding motif, so we first studied the relative energies of the isolated tautomers in the gas phase and in water, and then the geometries and stabilities of the single rosettes in both media. Because the outer amino groups do not participate in hydrogen bonds, and thus are not needed for assembly, we simplified our systems by replacing them with hydrogen atoms. In addition, to produce rosettes or nanowires exclusively, it is a current experimental procedure to replace them with long alkylic chains.[1,10] Therefore, one may wonder if this change could affect the relative stability of the monomeric units. Our results showed the same trend whether there is a hydrogen atom or an NH_2 group (see Table 1). The energy differences between the amino–imine tautomers are significant, both in the gas phase and in water: up to 27 and 15 kcal mol^{-1}, respectively. This is consistent with experimental findings that the imino-like tautomers of some related compounds must be obtained by using a considerable amount of energy, such as UV radiation.[22,23]

Table 1. Relative energies [kcal mol^{-1}] of tautomers.

Monomer	Gas phase		Water	
	R = H	R = NH_2	R = H	R = NH_2
M	0.0	0.0	0.0	0.0
M′	24.0	23.1	13.2	12.7
M′′	27.6	31.5	15.2	17.6
a-AM	0.0	0.0	7.5	8.2
a-AM′	2.3	0.8	0.0	0.0
b-AM	0.6	0.0	7.4	8.2
b-AM′	13.1	18.7	3.7	6.9

For AM, our results are in line with previous computations in the gas phase.[12a,c] However, the energetic preference of its hydroxy or carbonyl tautomers has been under debate since the 1950s[24] due to the lack of data in the solid state. It has been shown that the preference for a specific tautomer will depend whether they are found in the solid state or in solution.[25] Our computations show that the energy difference between the *a*-AM (enol form) and *a*-AM′ (first keto form, protonated at position 1, as shown in Scheme 1) is very small, and this is consistent with the fact that they may coexist in solution.[12a] The next keto form (*b*-AM′), is 13.1 and 3.7 kcal mol^{-1} less stable in the gas phase and in water, respectively. However, in water, the relative stabilities of AM tautomers are surprisingly reversed. In aqueous media, *a*-AM′ is now the most stable tautomer and *a*-AM or *b*-AM are less stable. There is some experimental evidence of ammeline tautomers in the solid state,[24a,b] however, the tautomeric equilibrium of this compound in solution is still unknown.

Now we address the situation in the rosettes. The molecular structures without symmetry restrictions are shown in Figures 1 and 2, and the bonding energy analysis in the gas phase is presented in Table 2 (geometrical parameters are shown in Table S1 in the Supporting Information). It is interesting to note that two molecules could give rise to seven different rosettes with different electronic structures. If we consider the hydrogen atoms of the inner and outer hydrogen-bond donors, it can be noted that the structures with prime labels are the result of moving a proton from one atom to another (Schemes 2 and 3), that is, an intermolecular proton transfer from amine to imine forms (M→M′ or M″) and from enol to keto forms (*a*-AM→*a*-AM′, or *b*-AM→*b*-AM′). More interestingly, AM could form two different rosettes depending on the orientation of the -OH group, which could lead to two different functionalities with the same molecule. In Figures 1 and 2, note that neither of the global minima are completely planar. They adopt a C_2-symmetric structure, except for *a*-AM_6, which assumes a S_6-symmetric arrangement. For example, there are three general shapes: saddle-like shapes (M_6, *a*-AM_6, and *a*-AM'_6), bowl-like shapes (*b*-AM_6 and *b*-AM'_6), and irregular or almost-planar structures (M'_6 and M''_6). The energy needed to make them planar ($\Delta E_{C_1 \rightarrow C_s}$) is very low, as shown in Table 2, so it could be easily compensated in a stacking environment due to π–π interactions, or over a surface due to adsorption effects. These results also justify all the analysis of the planar systems.

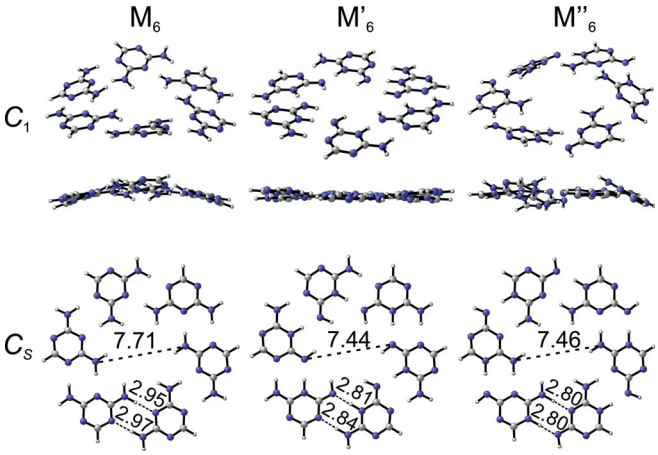

Figure 1. Global minima of M rosette-like structures and C_s structures with hydrogen-bond lengths [Å]. Calculated at the ZORA-BLYP-D3(BJ)/TZ2P level.

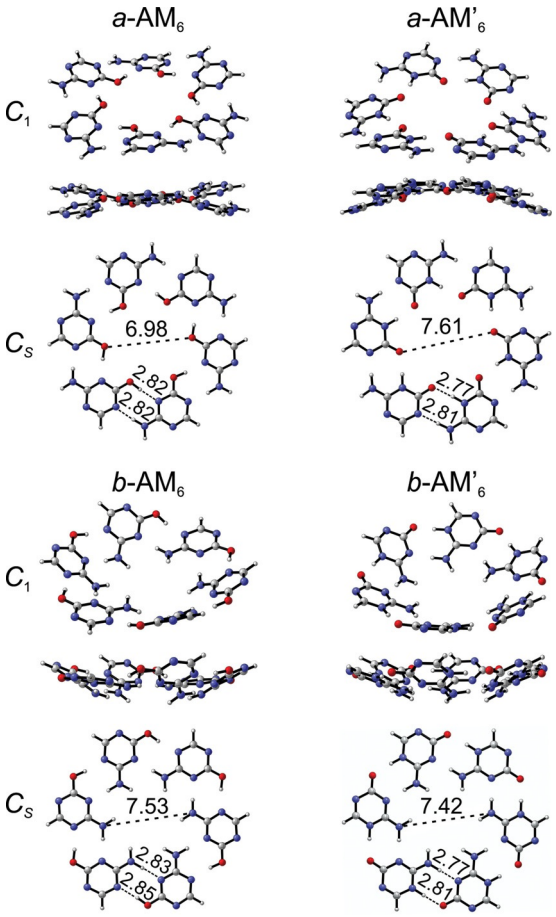

Figure 2. Global minima of AM rosette-like structures and C_s structures with hydrogen-bond lengths [Å]. Calculated at the ZORA-BLYP-D3(BJ)/TZ2P level.

Table 2. Analysis of the bonding energies of rosettes in the gas phase (calculated at the ZORA-BLYP-D3(BJ)/TZ2P level of theory).

Rosette	ΔG_f[a] [kcal mol^{-1}]	ΔE_f[b] [kcal mol^{-1}]	ΔE_{taut}[c] [kcal mol^{-1}]	ΔE_{bond}[d] [kcal mol^{-1}]	$\Delta E_{bond}^{C_s}$[e] [kcal mol^{-1}]	$\Delta E_{C_1 \rightarrow C_s}$[f] [kcal mol^{-1}]
M_6	−2.8	−80.3	0.0	−80.3	−79.3	1.0
M'_6	40.4	−36.3	143.8	−180.1	−180.1	0.0
M''_6	58.8	−16.6	165.5	−182.1	−178.9	3.2
a-AM_6	−30.9	−102.5	0.0	−102.5	−101.5	1.0
a-AM'_6	−57.1	−128.4	13.7	−142.2	−141.8	0.3
b-AM_6	−14.6	−86.3	0.0	−90.0	−85.5	4.5
b-AM'_6	−21.1	−90.9	78.5	−169.4	−163.1	6.3

[a] Gibbs free energy of formation of nonsymmetric minima. [b] Formation energy. [c] Tautomerization energy. [d] Bonding energy. [e] Planar bond energy. [f] Planarization energy [Eqs. (1–4)].

Although the bonding energies are much larger for the prime-labeled systems, the relative stability of the rosettes is defined by the Gibbs free energy of formation and the formation energy. For M'_6 and M''_6, we see that the tautomerization energy required to get the imine-like structures is very large (see Tables 1 and 2). Thus, M_6 is the most energetically favored because there is no energetic cost for tautomerization. Although the most stable structure of AM is either *a*-AM or *b*-AM in the gas phase, the formation energies (ΔG_f and ΔE_f) indicate that the most stable rosette is *a*-AM'_6. Even the rosette of the least-stable tautomer, *b*-AM'_6, is more strongly bound than *b*-AM_6 and *a*-AM'_6, but again, the tautomerization energy counterbalances the overall energy. Below we will show the interplay of the cooperativity.

Finally, when we put the systems in water the differences are stressed. The formation energies in water (see Table 3) sug-

Table 3. Analysis of the formation energies of rosettes with C_{2h} symmetry in water. (calculated at the ZORA-BLYP-D3(BJ)/TZ2P level of theory).

Rosette	ΔE_f^w [kcal mol^{-1}]	ΔE_{taut}^w [kcal mol^{-1}]	ΔE_{bond}^w [kcal mol^{-1}]
M_6	−44.3	0.0	−44.3
M'_6	1.6	78.9	−77.3
M''_6	16.6	91.3	−74.7
a-AM_6	−23.3	44.6	−67.9
a-AM'_6	−63.8	0.0	−63.8
b-AM_6	−15.3	44.7	−60.0
b-AM'_6	−40.5	22.0	−62.6

gest that only two systems will prevail in solution: M_6 and *a*-AM'_6, although *b*-AM'_6 could coexist or compete with the latter. Although the ΔE_f^w values for M'_6 and M''_6 are positive, we have to note that the bonding energies indicate that they are stable systems. Therefore, unless we provide them with the energy needed to overcome the tautomerization barrier, the imine-like rosettes are not accessible.

2.2. Cooperativity in the Gas Phase

In previous works on guanine[26] and cyanuric acid[27] cyclic complexes, we showed that when all the hydrogen bonds point in the same direction, they experience a large synergetic effect. The origin of this cooperativity is the charge separation that occurs due to donor–acceptor interactions in the σ-electron system from monomer to monomer.[26] Herein, when considering the proton transfer in the amino→imine (M→M′ or M″) and enol→keto (*a*-AM→*a*-AM′, or *b*-AM→*b*-AM′) tautomerisms, cooperativity shows up. Consequently, the prime-labeled systems show a larger bonding energy than their amino (M) and enol counterparts (*a*-AM_6 and *b*-AM_6), as shown in Table 4. However, there are two energy penalties that will have an impact on the formation energy. First, the most stable monomers must overcome the tautomerization energy, as shown in Table 2. The second penalty is the energy needed to deform the isolated tautomers to the geometry they will acquire in the rosette. In Table 4, it can be seen that the preparation energy (deformation) is also larger for imine tautomers and much lower for the keto forms of AM.

The interplay between cooperativity, tautomerization, and preparation energy determine the final outcome. Therefore, ammeline is the only case in which the tautomerization energy of the first keto form (*a*-AM'_6) is sufficiently low to be overcome by the large synergy. For example, the synergy of *b*-AM'_6 is 15 kcal mol^{-1} greater than that of *a*-AM'_6, but again the former has to pull against big tautomerization and preparation energies. Because *a*-AM'_6 is the most stable rosette in both the gas phase and water, which also has the additional factor of a large cooperativity effect, AM seems to be a better candidate than M for the design of self-assembling rosettes.

2.3. Energy Decomposition Analysis

Ammeline is the first hydrolysis product of melamine. Thus, the main difference between M_6 and *a*-AM_6/*b*-AM_6 is just one functional group, -NH_2 in the former and -OH in the latter. Although there is almost zero cooperativity in *a*-AM_6 and *b*-AM_6, these rosettes are more strongly bound than M_6. For example, the bonding energy difference between M_6 and *a*-AM_6 is 22.2 kcal mol^{-1}, and between M_6 and *b*-AM_6 the difference is 6.2 kcal mol^{-1} (see Table 4). The ΔE_{int} value for the dimers is also larger for AM (see also Table 4). Because cooperativity is not such an important factor, as it is in guanine and xanthine quartets,[26] this difference can only be explained on the basis of the pair-interaction energies and their individual energy contributions.

As we saw, the energy of formation of the dimers is important in determining the stabilization of the rosette, so we computed the interaction energy profiles for the most stable dimers in the gas phase (M_2, *a*-AM_2, and *b*-AM_2), which contain benzenoid-type rings and are comparable electronically. A potential energy surface scan was performed over the hydrogen-bond lengths according to the procedure presented in Ref. [28]. Then we decomposed the ΔE_{int} value in every step into physically meaningful energy terms that contribute to the hydrogen-bond energy: electrostatic, steric interactions, and covalence. The results are plotted in Figure 3.

Both AM dimers show stronger pair-interaction energies than M over the same distances. Although the differences between the attractive terms are almost negligible, M_2 shows a stronger electrostatic contribution but *a*-AM_2 shows a greater orbital component. However, the decisive factor is the Pauli repulsion. Despite some small variations, these findings are in line with previous results for similar systems,[28] in which Pauli repulsion determines the hydrogen-bond strength.

Table 4. Analysis of the bonding energies of rosettes in the gas phase (calculated at the ZORA-BLYP-D3(BJ)/TZ2P level of theory).

Rosette	ΔE_{bond}^{Cs} [kcal mol^{-1}]	ΔE_{prep} [a] [kcal mol^{-1}]	ΔE_{int} [b] [kcal mol^{-1}]	ΔE_{pair} [c] [kcal mol^{-1}]	ΔE_{diag} [d] [kcal mol^{-1}]	ΔE_{front} [e] [kcal mol^{-1}]	ΔE_{syn} [f] [kcal mol^{-1}]
M_6	−79.3	7.4	−86.8	−14.3	0.0	0.1	−1.8
M'_6	−180.1	24.6	−204.7	−21.5	−2.4	−1.2	−57.8
M''_6	−178.9	33.5	−212.4	−22.2	−1.8	−0.8	−66.2
a-AM_6	−101.5	19.2	−120.7	−19.7	−0.1	0.0	−1.9
a-AM'_6	−141.8	19.3	−161.1	−17.4	−1.7	−0.8	−44.6
b-AM_6	−85.5	15.6	−101.1	−16.8	0.4	0.4	−3.7
b-AM'_6	−163.1	25.7	−188.8	−19.5	−1.7	−0.7	−59.8

[a] Preparation energy. [b] Interaction energy [Eq. (4)]. [c] Pair interaction. [d] Diagonal interaction. [e] Frontal interaction. [f] Synergy [Eqs. (7) and (8)].

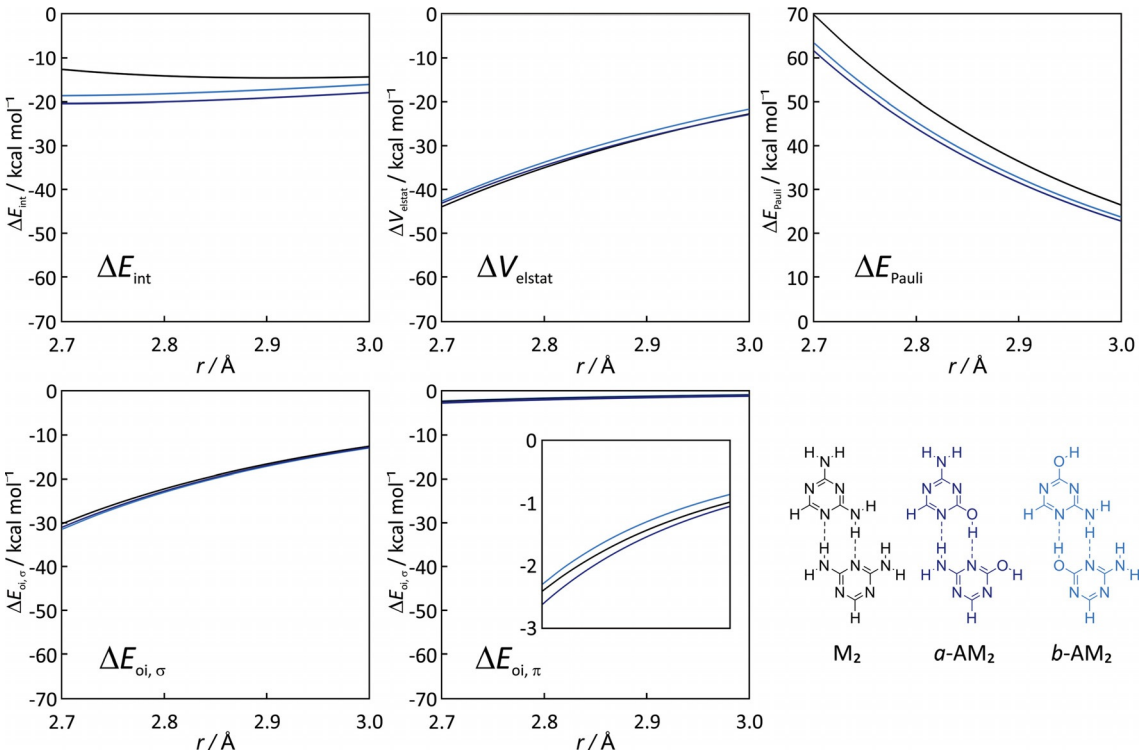

Figure 3. Decomposed energy terms [kcal mol^{-1}] as a function of the hydrogen-bond length r [Å] for M_2, a-AM_2, and b-AM_2. The dimers were optimized along constrained hydrogen-bond lengths at the BLYP-D3(BJ)/TZ2P level of theory.

2.4. Source and Mechanism of Cooperativity

Finally, to explore the basis of the cooperativity mechanism of M and AM rosettes, we used the same approach as for four-membered rosettes of guanine[26] and *N*-halo-guanine.[29] The method consists of the construction of the rosette starting from the monomer, and stepwise addition of more monomers to complete the cycle, as shown in Scheme 6. This also allows us to investigate whether the source of cooperativity in these rosettes is similar to that in the guanine quartets.

Therefore, we decomposed the interaction energy in each step, then computed the synergy in each energy component by applying Equations (6) and (7) in the Computational Methods Section. To illustrate this, the synergy in the electrostatic component of a-AM′$_6$ is computed as follows [Eq. (9)]:

$$\Delta E_{\mathrm{syn,elstat}} = \left[\sum_{n=1}^{5} \Delta V_{\mathrm{elstat}}(a\text{–}\mathrm{AM}'_{n+1})\right] - \left(6\,\Delta V_{\mathrm{elstat,pair}} + 6\,\Delta V_{\mathrm{elstat,diag}} + 6\,\Delta V_{\mathrm{elstat,front}}\right) \quad (9)$$

Results for a-AM′$_{n+1}$, the rosette with the largest formation energy, are presented in Table 5. The values for M′$_{n+1}$, M″$_{n+1}$, and b-AM′$_{n+1}$ are collected in Tables S2–S4. From Table 5, we can infer that every component increases progressively with the addition of monomers due to the cooperativity phenomenon. The interaction energy per added monomer increases from −17.4 to −30.5 kcal mol^{-1}, a strengthening of 13.1 kcal mol^{-1}. The addition of the last monomer leads to the formation of two pairs of hydrogen bonds, which correspond to a ΔE_{int} value of −31.4 kcal mol^{-1} per molecular unit.

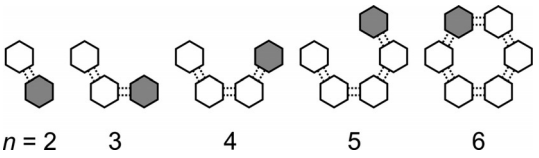

Scheme 6. Formation of the rosette in five steps by a stepwise addition of monomers (m) in one-way direction: $m_n + m$ ($n = 1, 2, 3, 4, 5$). Grey hexagons represent the incoming m.

Table 5. Energy decomposition for the formation of a-AM′$_{n+1}$ from a-AM′$_n$ + a-AM′ in a stepwise one-way direction ($n = 1, 2, 3, 4, 5$).

$n+1$	ΔE_{int} [kcal mol^{-1}]	$\Delta V_{\mathrm{elstat}}$ [kcal mol^{-1}]	$\Delta E_{\mathrm{Pauli}}$ [kcal mol^{-1}]	ΔE_{oi} [kcal mol^{-1}]		ΔE_{disp} [kcal mol^{-1}]
				ΔE_{σ}	ΔE_{π}	
1+1	−17.4	−30.6	36.6	−17.3	−1.8	−4.4
2+1	−23.9	−35.7	37.5	−19.1	−2.2	−4.5
3+1	−26.8	−37.9	37.8	−19.8	−2.4	−4.5
4+1	−30.5	−40.7	37.9	−20.4	−2.7	−4.5
5+1	−62.7	−75.1	73.4	−44.8	−7.3	−8.9
ΔE_{syn}	−44.6	−24.9	3.5	−17.5	−5.7	0.0

The energy decomposition analysis shows that the synergy in these rosettes is composed of 52% electrostatic and 36 and 12% orbital interactions in the σ- and π-electron systems, respectively. The same behavior is observed in M′$_6$, M″$_6$, and b-AM′$_6$ (see Tables S2–S4). However, their synergy in the σ-elec-

tron system is even greater: −21.9, −26.5, and −22.1 kcal mol^{-1} respectively.

The mechanism of the cooperativity is reexamined and explained by analyzing the charge redistribution within the construction shown in Scheme 6. The pair formation leads to donor–acceptor orbital interactions between lone-pair (LP) orbitals and N–H antibonding acceptor orbitals: $\sigma_{LP} \rightarrow \sigma^*_{N-H}$. Throughout the stepwise addition of monomers, the charge separation gradually and monotonically increased, as shown in Figure 4 with the VDD atomic charges of the front atoms and

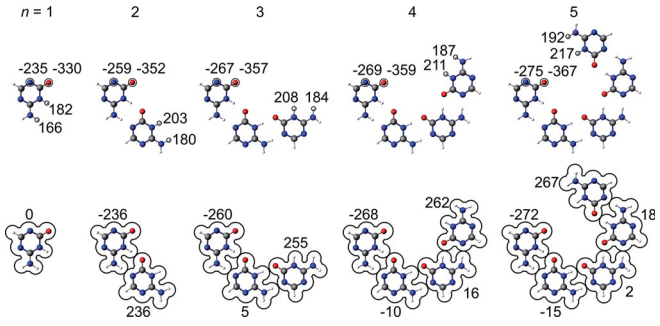

Figure 4. Top: VDD atomic charges [milli-a.u.] of the front atoms of *a*-AM′$_n$, in the geometry they adopt in the C_{2h}-symmetric orbitals. Bottom: Total VDD charges of *a*-AM′$_n$.

the total VDD charge of the monomers. The net charge on the frontier protons experienced an average increment of 17%, whereas the net charge of the hydrogen-bond acceptor atoms decreased by approximately 14%. Furthermore, monomers with hydrogen-bond acceptors became gradually more negatively charged and the monomers with hydrogen-bond donors became more positively charged. This has two consequences: 1) it improves the electrostatic attraction with additional monomers and 2) the LP σ_{HOMO} orbital of the hydrogen-bond acceptor is destabilized and goes up in energy and, in contrast, the antibonding σ_{LUMO} orbital of the hydrogen-bond donor is stabilized, as shown in Figure 5. As a consequence, the σ_{HOMO} and σ_{LUMO} orbitals become better partners for donor–acceptor interactions each time a monomer is added to the rosette.

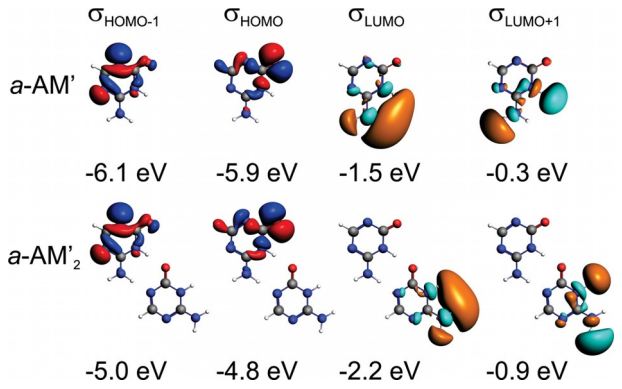

Figure 5. Oxygen (σ_{HOMO}), nitrogen lone-pair orbitals (σ_{HOMO-1}), and N–H unoccupied orbitals (σ_{LUMO} and σ_{LUMO+1}) and the energies [eV] of the front atoms of *a*-AM′ and *a*-AM′$_2$. Calculated at the ZORA-BLYP-D3(BJ)/TZ2P level of theory. (See also Figures S1 and S2).

3. Conclusions

Herein we have given a theoretical background for design principles of supramolecular systems. Through our DFT-D calculations, we have pinpointed the factors that make ammeline a more robust building block than melamine for the construction of self-assembled rosettes. Our results show that the most stable structures in the gas phase and in water are those of melamine in its amino-like form (M_6) and ammeline in its keto-like form (protonated at position 1, *a*-AM′). Unlike M, the most stable rosettes of AM show great synergy effects and thus strong binding energies. Additionally, AM also displays larger pair interactions. Therefore, these positive factors can be exploited by chemists in noncovalent synthesis approaches. Furthermore, if it is experimentally possible to control the selectivity of both keto forms of AM rosettes, our results show that it would be possible to obtain two materials with different properties.

The mechanism of the cooperativity phenomenon was proven to be the same as that in guanine and *N*-halo-guanine quartets; namely, the charge separation in the σ electronic system caused by donor–acceptor interactions between the lone pairs on the proton acceptor and the unoccupied orbitals on the proton-donor groups. This charge separation is the mechanism for the enhancement of the electrostatic interaction and the σ-orbital interactions. In the rosettes studied herein, the electrostatic component represents an average contribution of 50% of the total synergy, whereas the σ and π orbital interactions contribute 40 and 10% to the synergy, respectively. Our findings prove that synergy can be used as a tool to improve self-assembly in supramolecular chemistry.

Acknowledgements

We thank the Netherlands Organization for Scientific Research (NWO/CW) for financial support. A.N.P. thanks the National Scientific and Technical Research Council (CONICET), Argentina, for a doctoral fellowship.

Conflict of Interest

The authors declare no conflict of interest.

Keywords: cooperative effects · hydrogen bonds · rosettes · self-assembly · supramolecular chemistry

[1] a) S. I. Stupp, L. C. Palmer, *Chem. Mater.* **2014**, *26*, 507–518; b) M. J. Mayoral, N. Bilbao, D. González-Rodríguez, *ChemistryOpen* **2016**, *5*, 10–32; c) R. L. Beingessner, Y. Fan, H. Fenniri, *RSC Adv.* **2016**, *6*, 75820–75838; d) B. Adhikari, X. Lin, M. Yamauchi, H. Ouchi, K. Aratsu, S. Yagai, *Chem. Commun.* **2017**, *53*, 9663–9683.

[2] *Guanine Quartets: Structure and Application*, (Eds.: W. Fritzsche, L. Spindler), RSC Publishing, Cambridge, **2012**.

[3] a) A. Kohlmeier, L. Vogel, D. Janietz, *Soft Matter* **2013**, *9*, 9476–9486; b) L. Niu, J. Song, J. Li, N. Tao, M. Lu, K. Fan, *Soft Matter* **2013**, *9*, 7780; c) V. Venkatesh, N. K. Mishra, I. Romero-Canelón, R. R. Vernooij, H. Shi, J. P. C. Coverdale, A. Habtemariam, S. Verma, P. J. Sadler, *J. Am. Chem. Soc.* **2017**, *139*, 5656–5659.

[4] A. P. H. J. Schenning, P. Jonkheijm, F. J. M. Hoeben, J. Van Herrikhuyzen, S. C. J. Meskers, E. W. Meijer, L. M. Herz, C. Daniel, C. Silva, R. T. Phillips, R. H. Friend, D. Beljonne, A. Miura, S. De Feyter, M. Zdanowska, H. Uji-i, F. C. De Schryver, Z. Chen, F. Würthner, M. Mas-Torrent, D. den Boer, M. Durkut, P. Hadley, *Synth. Met.* **2004**, *147*, 43 – 48.

[5] H. Diem, G. Matthias, R. A. Wagner in *Amino Resins. Ullmann's Encyclopedia of Industrial Chemistry*, Wiley-VCH Verlag GmbH & Co. KGaA, Weinheim, Germany, **2010**.

[6] B. Roy, P. Bairi, A. K. Nandi, *RSC Adv.* **2014**, *4*, 1708.

[7] a) P. A. Staniec, L. M. A. Perdigão, B. L. Rogers, N. R. Champness, P. H. Beton, *J. Phys. Chem. C* **2007**, *111*, 886 – 893; b) W. Xu, M. Dong, H. Gersen, E. Rauls, S. Vázquez-Campos, M. Crego-Calama, D. N. Reinhoudt, I. Stensgaard, E. Laegsgaard, T. R. Linderoth, F. Besenbacher, *Small* **2007**, *3*, 854 – 8; c) F. Silly, A. Q. Shaw, M. R. Castell, G. A. D. Briggs, M. Mura, N. Martsinovich, L. Kantorovich, *J. Phys. Chem. C* **2008**, *112*, 11476 – 11480; d) M. Mura, N. Martsinovich, L. Kantorovich, *Nanotechnology* **2008**, *19*, 465704; e) H. Zhang, Z. Xie, L. Long, H. Zhong, W. Zhao, B.-W. Mao, X. Xu, L.-S. Zheng, *J. Phys. Chem. C* **2008**, *111*, 4209 – 4218.

[8] a) H.-M. Zhang, Z.-K. Pei, Z.-X. Xie, L.-S. Long, B.-W. Mao, X. Xu, L.-S. Zheng, *J. Phys. Chem. C* **2009**, *113*, 13940 – 13946; b) A. Ciesielski, S. Haar, G. Paragi, Z. Kupihár, Z. Kele, S. Masiero, C. Fonseca Guerra, F. M. Bickelhaupt, G. P. Spada, L. Kovács, P. Samorì, *Phys. Chem. Chem. Phys.* **2013**, *15*, 12442.

[9] a) N. Katsonis, H. Xu, R. M. Haak, T. Kudernac, Ž. Tomović, S. George, M. Van Der Auweraer, A. P. H. J. Schenning, E. W. Meijer, B. L. Feringa, S. De Feyter, *Angew. Chem. Int. Ed.* **2008**, *47*, 4997 – 5001; *Angew. Chem.* **2008**, *120*, 5075 – 5079; b) A. Minoia, Z. Guo, H. Xu, S. J. George, A. P. H. J. Schenning, S. De Feyter, R. Lazzaroni, *Chem. Commun.* **2011**, *47*, 10924 – 10926.

[10] a) P. Jonkheijm, A. Miura, M. Zdanowska, F. J. M. Hoeben, S. De Feyter, A. P. H. J. Schenning, F. C. De Schryver, E. W. Meijer, *Angew. Chem. Int. Ed.* **2004**, *43*, 74 – 78; *Angew. Chem.* **2004**, *116*, 76 – 80; b) K. E. Maly, C. Dauphin, J. D. Wuest, *J. Mater. Chem.* **2006**, *16*, 4695.

[11] S. Yagai, S. Mahesh, Y. Kikkawa, K. Unoike, T. Karatsu, A. Kitamura, A. Ajayaghosh, *Angew. Chem.* **2008**, *120*, 4769 – 4772.

[12] a) Y. Wang, C. U. Pittman, Jr., S. Saebo, *J. Org. Chem.* **1993**, *58*, 3085 – 3090; b) Y. H. Jang, S. Hwang, S. B. Chang, J. Ku, D. S. Chung, *J. Phys. Chem. A* **2009**, *113*, 13036 – 13040; c) M. Hatanaka, *J. Phys. Chem. A* **2015**, *119*, 1074 – 1086.

[13] a) F. M. Bickelhaupt, E. J. Baerends, in *Reviews in Computational Chemistry, Vol. 15* (Eds.: K. B. Lipkowitz, D. B. Boyd), Wiley-VCH, New York, **2000**, pp. 1 – 86; b) R. Stowasser, R. Hoffmann, *J. Am. Chem. Soc.* **1999**, *121*, 3414 – 3420; c) E. J. Baerends, O. V. Gritsenko, R. Van Meer, *Phys. Chem. Chem. Phys.* **2013**, *15*, 16408 – 16425.

[14] T. Ziegler, A. Rauk, *Inorg. Chem.* **1979**, *18*, 1558 – 1565.

[15] C. Fonseca Guerra, J.-W. Handgraaf, E. J. Baerends, F. M. Bickelhaupt, *J. Comput. Chem.* **2004**, *25*, 189 – 210.

[16] a) G. te Velde, F. M. Bickelhaupt, E. J. Baerends, S. J. A. van Gisbergen, C. Fonseca Guerra, J. G. Snijders, T. Ziegler, *J. Comput. Chem.* **2001**, *22*, 931 – 967; b) E. J. Baerends, T. Ziegler, J. Autschbach, D. Bashford, A. Bérces, F. M. Bickelhaupt, C. Bo, P. M. Boerrigter, L. Cavallo, D. P. Chong, L. Deng, R. M. Dickson, D. E. Ellis, M. van Faassen, L. Fan, T. H. Fischer, C. Fonseca Guerra, A. Ghysels, A. Giammona, S. J. A. van Gisbergen, A. W. Gçtz, J. A. Groeneveld, O. V. Gritsenko, M. Grüning, S. Gusarov, F. E. Harris, P. van den Hoek, C. R. Jacob, H. Jacobsen, L. Jensen, J. W. Kaminski, G. van Kessel, F. Kootstra, A. Kovalenko, M. V. Krykunov, E. van Lenthe, D. A. McCormack, A. Michalak, M. Mitoraj, J. Neugebauer, V. P. Nicu, L. Noodleman, V. P. Osinga, S. Patchkovskii, P. H. T. Philipsen, D. Post, C. C. Pye, W. Ravenek, J. I. Rodríguez, P. Ros, P. R. T. Schipper, G. Schreckenbach, J. S. Seldenthuis, M. Seth, J. G. Snijders, M. Solà, M. Swart, D. Swerhone, G. te Velde, P. Vernooijs, L. Versluis, L. Visscher, O. Visser, F. Wang, T. A. Wesolowski, E. M. van Wezenbeek, G. Wiesenekker, S. K. Wolff, T. K. Woo, A. L. Yakovlev, ADF2014.01, SCM, Theoretical Chemistry, Vrije Universiteit, Amsterdam, The Netherlands, http://www.scm.com.

[17] a) S. Grimme, J. Antony, S. Ehrlich, H. Krieg, *J. Chem. Phys.* **2010**, *132*, 154104; b) S. Grimme, S. Ehrlich, L. Goerigk, *J. Comput. Chem.* **2011**, *32*, 1456 – 1465; c) S. Grimme, *J. Comput. Chem.* **2004**, *25*, 1463 – 1473; d) S. Grimme, *J. Comput. Chem.* **2006**, *27*, 1787 – 1799.

[18] a) C. Fonseca Guerra, T. van der Wijst, J. Poater, M. Swart, F. M. Bickelhaupt, *Theor. Chem. Acc.* **2010**, *125*, 245 – 252; b) T. van der Wijst, C. Fonseca Guerra, M. Swart, F. M. Bickelhaupt, B. Lippert, *Angew. Chem. Int. Ed.* **2009**, *48*, 3285 – 3287; *Angew. Chem.* **2009**, *121*, 3335 – 3337.

[19] a) Y. Connolly Martin, *J. Comput. Aided. Mol. Des.* **2009**, *23*, 693 – 704; b) R. A. Sayle, *J. Comput. Aided. Mol. Des.* **2010**, *24*, 485 – 496.

[20] a) T. H. Rehm, C. Schmuck, *Chem. Soc. Rev.* **2010**, *39*, 3597; b) M. Ma, D. Bong, *Langmuir* **2011**, *27*, 8841 – 8853; c) B. J. Cafferty, I. Gállego, M. C. Chen, K. I. Farley, R. Eritja, N. V. Hud, *J. Am. Chem. Soc.* **2013**, *135*, 2447 – 2450.

[21] a) A. Klamt, G. Schüürmann, *J. Chem. Soc. Perkin Trans. 2* **1993**, *5*, 799; b) A. Klamt, *J. Phys. Chem.* **1995**, *99*, 2224; c) C. C. Pye, T. Ziegler, *Theor. Chem. Acc.* **1999**, *101*, 396.

[22] N. Akai, T. Harada, K. Shin-ya, K. Ohno, M. Aida, *J. Phys. Chem. A* **2006**, *110*, 6016 – 6022.

[23] I. Reva, M. J. Nowak, L. Lapinski, R. Fausto, *J. Phys. Chem. B* **2012**, *116*, 5703 – 5710.

[24] a) W. M. Padgett, W. F. Hamner, *J. Am. Chem. Soc.* **1958**, *80*, 803 – 808; b) B. V. Lotsch, W. Schnick, *Z. Anorg. Allg. Chem.* **2006**, *632*, 1457 – 1464.

[25] P. V. Bernhardt, E. J. Hayes, *Inorg. Chem.* **1998**, *37*, 4214 – 4219.

[26] a) C. Fonseca Guerra, H. Zijlstra, G. Paragi, F. M. Bickelhaupt, *Chem. Eur. J.* **2011**, *17*, 12612 – 12622; b) G. Paragi, C. Fonseca Guerra, *Chem. Eur. J.* **2017**, *23*, 3042 – 3050.

[27] A. N. Petelski, N. M. Peruchena, S. C. Pamies, G. L. Sosa, *J. Mol. Model.* **2017**, *23*, 263.

[28] S. C. C. van der Lubbe, C. Fonseca Guerra, *Chem. A Eur. J.* **2017**, *23*, 10249 – 10253.

[29] L. P. Wolters, N. W. G. Smits, C. Fonseca Guerra, *Phys. Chem. Chem. Phys.* **2015**, *17*, 1585 – 1592.

Received: October 10, 2018
Revised manuscript received: October 25, 2018

